Improved WSR-88D Scanning Strategies for Convective Storms

RODGER A. BROWN AND VINCENT T. WOOD

National Severe Storms Laboratory, Norman, Oklahoma

DALE SIRMANS

System Technology Associates, Inc., Norman, Oklahoma

(Manuscript received 13 May 1999, in final form 29 November 1999)

ABSTRACT

The Weather Surveillance Radar-1988 Doppler (WSR-88D) is an important operational and research tool for detecting and monitoring convective storms. Two scanning strategies, or volume coverage patterns, VCP 11 and 21, are used in storm situations. Users find that these original VCPs do not always provide the vertical or temporal resolution that is desired. To help solve these resolution problems, a procedure is proposed for developing optimized and flexible VCPs. A VCP is *optimized* when the maximum height uncertainty (expressed in percent of true height) is essentially the same at all ranges and for all heights of storm features. A VCP becomes *flexible* when the volume scan terminates and recycles after it tilts above all radar return or reaches a specified elevation angle. Two sample VCPs, which are optimized and flexible, are presented, and simulated radar data show that they perform better than the current VCPs.

1. Introduction

Currently, there are two Weather Surveillance Radar-1988 Doppler (WSR-88D) scanning strategies, or volume coverage patterns (VCPs), that are used to detect and monitor convective storms. VCP 11 consists of 14 elevation scans (0.5°–19.5°) in 5 min and VCP 21 consists of 9 scans (also 0.5°–19.5°) in 6 min (OFCMSSR 1991). Neither VCP does well in resolving characteristics of storm features beyond about 150 km. For storms that extend above 5° elevation angle, VCP 11 is vastly superior to VCP 21 owing to enhanced vertical resolution in the upper portion of storms (e.g., Brown et al. 2000). Within roughly 25 km of the radar, neither VCP detects the upper portions of storms owing to the ''cone of silence'' represented by the absence of measurements above 19.5° elevation.

Weather forecasters and other WSR-88D users have been lobbying for improved vertical and temporal resolution. There is a need for better vertical resolution at lower elevation angles to improve precipitation estimates during all seasons and to improve detection and monitoring of features associated with distant and shallow convective storms. Furthermore, data collection at higher elevation angles is needed to improve detection and monitoring of storm tops and other storm features, especially those close to the radar. Also, improved temporal resolution would better detect and monitor rapidly evolving downbursts and tornadoes associated with severe thunderstorms and hurricanes.

The vertical extent of radar detection can be increased by increasing the maximum elevation angle from 19.5° to 60°, the maximum permitted by the radar system. In order to improve the vertical resolution, one would like to have a VCP that has elevation angles closest together at far ranges (i.e., at the lower elevation angles), while maintaining the same relative height intervals between successive elevation angles at closer ranges. Vertical resolution can be improved by creating a set of ''optimized'' elevation angles where, for example, the height difference between successive elevation angles at a given height is the same at all ranges, and the height difference at a given height is proportional to height above the ground.

Two approaches are proposed here to improve temporal resolution. One approach is to increase the rotation rate to near the maximum rate (five revolutions per minute or 30° s^{-1}) while transmitting a sufficient number of pulses to maintain specified reflectivity and velocity accuracy (1 dB*Z* and 1 m s^{-1}, respectively). The second approach is to use a technique developed for selected WSR-57 radars in the 1970s and 1980s (e.g., Saffle 1976; Greene et al. 1983). After the radar has completed a minimum number of elevation angle scans, the volume

Corresponding author address: Dr. Rodger A. Brown, National Severe Storms Laboratory, 1313 Halley Circle, Norman, OK 73069. E-mail: brown@nssl.noaa.gov

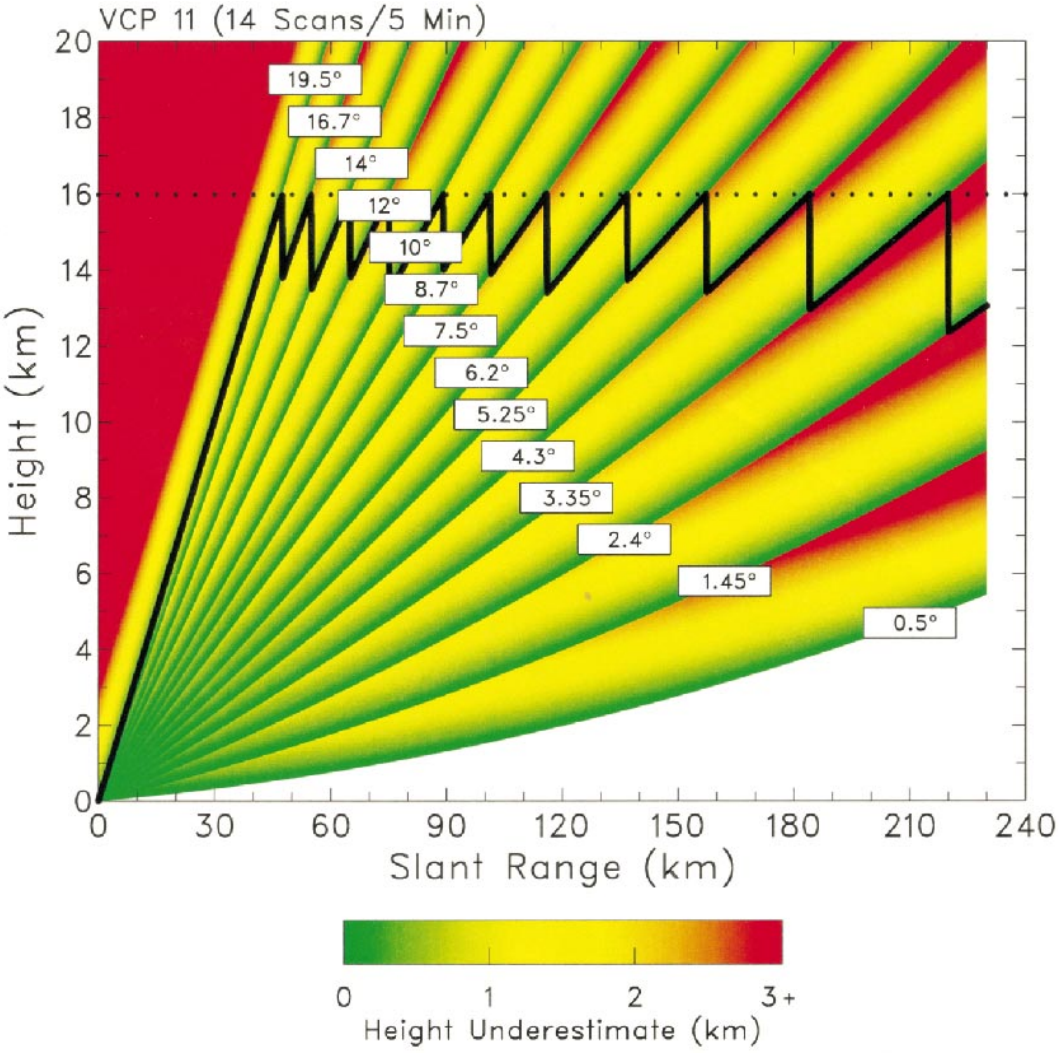

FIG. 1. Height of VCP 11 elevation angles as a function of slant range. The center of the radar beam lies along the labeled line (boundary between red and green). The height of a storm feature (such as the dotted line at 16-km height) that lies between two elevation angles is determined by the lower elevation angle, and therefore, the true height is underestimated by the amount indicated by the colored bands (along the dotted line). Height underestimation also is represented by the black jagged line that depicts the variation of apparent height (i.e., the center of the highest elevation angle with radar return) as a function of range.

scan is terminated as soon as two consecutive elevation angles are detected that have no radar return above a given threshold value, rather than continuing the scan through the highest elevation angle. The volume scan also could be terminated at an elevation angle specified by the radar operator.

The types of improvements that are proposed cannot be implemented immediately because some of the algorithms need to be modified in order to accommodate changes in elevation angles and scanning time. Our discussion is limited to single WSR-88Ds that do not benefit from observations made by surrounding radars. Also, solutions for mountaintop radars, which require negative elevation angles to properly sample crucial weather phenomena, are not discussed.

2. Technique for optimizing VCPs

Plotted in Fig. 1 are the height underestimates associated with the elevation angles of VCP 11 [analogous to figures used by Howard et al. (1997)]. As an example of how to interpret the colored bands in the figure, assume that VCP 11 is used to detect the top of a 16-km-tall storm (dotted line) at a slant range of 230 km. The storm top is above the center of the 2.4° elevation beam but below the center of the 3.35° elevation beam. The highest elevation angle showing radar return is 2.4°, which represents an apparent storm top of 13 km at a range of 230 km. The red color at 16-km height indicates that, if the storm top were at 16 km, the radar would underestimate it by about 3 km.

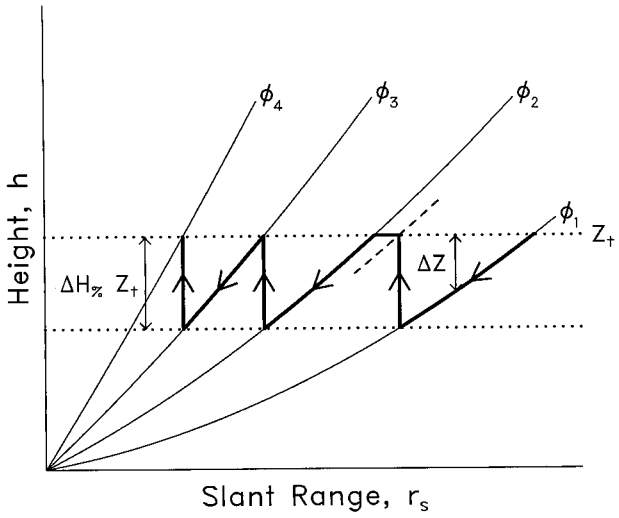

FIG. 2. Schematic of the process used to compute the elevation angles for an optimized VCP. See discussion in the text for details.

Superimposed on the elevation angles in Fig. 1 is a jagged black line that portrays height underestimates in a different form [analogous to curves used by Maddox et al. (1999)]. The jagged line depicts the variation of apparent height of a 16-km-tall storm (i.e., the center of the beam for the highest elevation angle with radar return) as a function of range associated with the VCP 11 scanning strategy. The jaggedness is somewhat erratic, and the vertical fluctuations generally increase with increasing range. It would be desirable to develop a scanning strategy where the vertical fluctuations are approximately uniform with range. In this way, maximum height uncertainties associated with a particular storm feature would be the same for all ranges (even though the resolution of the features would be degraded owing to the linearly widening beam with increasing range from the radar).

One approach for developing an optimized VCP would be to specify the maximum height underestimate desired (expressed as a percentage) and then compute the set of elevation angles that maintain the same maximum height underestimate. A procedure for doing this is illustrated in Fig. 2. First, one specifies the true height (Z_t); an intermediate height of 10 km was chosen for the development discussed here. Then, one selects a maximum height underestimate ($\Delta H_{\%}$) as a percentage of Z_t. Finally, the minimum elevation angle (ϕ_1) and maximum elevation angle are selected. Though a lower minimum elevation angle of 0.3° would be more desirable (Smith 1998), the current value of 0.5° was used. Since the WSR-88D was designed with a mechanical stop at 60° elevation, a maximum elevation angle of 58° was specified. The higher elevation angles are needed to document storm evolution over populated areas close to the radar.

The procedure to compute the angles is to start at the slant range where the height of the lowest elevation angle (ϕ_1) is equal to Z_t (the right edge of Fig. 2). With decreasing slant range (r_s) at that elevation angle, compute the height underestimate, $\Delta Z = Z_t - h$, where h is the height of the elevation angle at a given slant range. When ΔZ equals $\Delta H_{\%} \times Z_t$, return to Z_t and compute a new elevation angle (ϕ_2) that corresponds to that slant range and Z_t. If the difference between elevation angles is less than one-half beamwidth (the median WSR-88D one-way half-power beamwidth of 0.84° is used here), then decrease the range at the Z_t height until the elevation angle difference is equal to one-half beamwidth; this procedure is illustrated in Fig. 2 between ϕ_1 and ϕ_2. The equation for computing the new elevation angle is derived in appendix A. The process is repeated until the new ΔZ equals $\Delta H_{\%} \times Z_t$, and so on. In this way, a VCP is developed that has a consistent maximum height underestimate.

The elevation angles and cumulative scan times were computed for a reasonable range of maximum height underestimates. For these computations, the standard deviation of the power (reflectivity) estimate was constrained to be less than 1 dB, and the standard deviation of the Doppler velocity estimate was constrained to be less than about 1 m s^{-1} for the specified benchmark conditions of a signal-to-noise ratio greater than 8 dB and a spectrum width of 4 m s^{-1}. The maximum feasible rotation rates were determined from the relationships between standard deviation of the estimates and antenna rotation rate given in appendix B. Constraints were placed on spectral broadening and its impact on clutter filter performance, but the estimate standard deviation constraints proved to be dominant.

For elevation angles below 1.45°, the radar makes two complete (or contiguous surveillance) scans at each elevation angle to accommodate the ground clutter canceler and range unfolding of the Doppler waveform. For the first scan, in a contiguous surveillance mode, the antenna rotation rate is 3.5 revolutions per minute (rpm; 21° s^{-1}), which delivers a reflectivity standard deviation of 0.55 dB. For the second scan, in a contiguous Doppler mode, the rotation rate is 4.0 rpm (24° s^{-1}), which delivers a Doppler velocity standard deviation of 0.95 m s^{-1}. For the batch mode, between elevation angles of 1.45° and 7.0°, small groups of radar pulses are used alternatively to compute reflectivity and Doppler velocity. The rotation rate for batch mode is 4.5 rpm (27° s^{-1}), which delivers a reflectivity standard deviation of 0.64 dB and Doppler velocity standard deviation of 1.1 m s^{-1}. For the contiguous Doppler mode above 7.0°, the rotation rate is 4.8 rpm (28.8° s^{-1}), which delivers a reflectivity standard deviation of 0.65 dB and a Doppler velocity standard deviation of 1.0 m s^{-1} (see appendix B).

Consideration was given for the time it takes (a) for the antenna to rise to the next elevation angle and (b) for the various computations that are made as the antenna descends at the end of the volume scan. The approximate time was computed by multiplying the ele-

TABLE 1. Optimized VCPs (vertical columns) for various maximum height underestimates. Elevation angles (ϕ) are in degrees and scan times are in minutes and seconds.

	Max height underestimate (%)										
	18.0	19.0	20.0	21.0	22.0	23.0	24.0	25.0	26.0	27.0	28.0
Tilt 1 ϕ =	0.50	0.50	0.50	0.50	0.50	0.50	0.50	0.50	0.50	0.50	0.50
Scan time =	0 33	0 33	0 33	0 33	0 33	0 33	0 33	0 33	0 33	0 33	0 33
Tilt 2 ϕ =	0.92	0.92	0.92	0.92	0.92	0.92	0.92	0.92	0.92	0.92	0.92
Scan time =	1 06	1 06	1 06	1 06	1 06	1 06	1 06	1 06	1 06	1 06	1 06
Tilt 3 ϕ =	1.34	1.34	1.34	1.34	1.34	1.34	1.34	1.34	1.34	1.34	1.34
Scan time =	1 39	1 39	1 39	1 39	1 39	1 39	1 39	1 39	1 39	1 39	1 39
Tilt 4 ϕ =	1.81	1.84	1.87	1.91	1.94	1.97	2.00	2.04	2.07	2.11	2.15
Scan time =	1 53	1 53	1 53	1 53	1 53	1 53	1 53	1 53	1 53	1 53	1 53
Tilt 5 ϕ =	2.36	2.43	2.51	2.59	2.66	2.75	2.83	2.92	3.01	3.10	3.20
Scan time =	2 07	2 07	2 07	2 07	2 07	2 07	2 07	2 07	2 08	2 08	2 08
Tilt 6 ϕ =	3.01	3.14	3.27	3.41	3.56	3.72	3.88	4.05	4.23	4.42	4.61
Scan time =	2 21	2 21	2 21	2 21	2 22	2 22	2 22	2 22	2 22	2 23	2 23
Tilt 7 ϕ =	3.78	3.98	4.20	4.44	4.69	4.95	5.23	5.52	5.84	6.17	6.53
Scan time =	2 35	2 35	2 36	2 36	2 36	2 37	2 37	2 37	2 38	2 38	2 39
Tilt 8 ϕ =	4.70	5.01	5.35	5.71	6.10	6.52	6.97	7.46	7.99	8.56	9.18
Scan time =	2 50	2 50	2 51	2 51	2 51	2 52	2 52	2 52	2 53	2 54	2 55
Tilt 9 ϕ =	5.80	6.26	6.76	7.31	7.90	8.55	9.26	10.03	10.89	11.83	12.86
Scan time =	3 04	3 05	3 06	3 06	3 06	3 07	3 08	3 08	3 09	3 11	3 12
Tilt 10 ϕ =	7.14	7.80	8.52	9.32	10.21	11.19	12.28	13.48	14.84	16.35	18.05
Scan time =	3 19	3 20	3 20	3 21	3 22	3 23	3 25	3 25	3 27	3 29	3 31
Tilt 11 ϕ =	8.77	9.69	10.72	11.88	13.18	14.63	16.28	18.15	20.28	22.71	25.51
Scan time =	3 33	3 34	3 36	3 36	3 38	3 40	3 42	3 44	3 47	3 50	3 53
Tilt 12 ϕ =	10.76	12.04	13.48	15.13	17.02	19.19	21.68	24.56	27.96	31.96	36.77
Scan time =	3 48	3 50	3 52	3 53	3 56	3 59	4 02	4 05	4 09	4 14	4 21
Tilt 13 ϕ =	13.19	14.95	16.97	19.32	22.07	25.29	29.10	33.68	39.32	46.51	56.25
Scan time =	4 04	4 06	4 09	4 11	4 15	4 19	4 24	4 29	4 36	4 46	4 58
Tilt 14 ϕ =	16.18	18.59	21.42	24.77	28.81	33.72	39.81	47.69			
Scan time =	4 20	4 24	4 27	4 31	4 36	4 42	4 50	5 00			
Tilt 15 ϕ =	19.88	23.19	27.18	32.04	38.16	46.16	57.42				
Scan time =	4 38	4 42	4 47	4 53	5 01	5 11	5 26				
Tilt 16 ϕ =	24.51	29.10	34.83	42.20	52.41						
Scan time =	4 56	5 02	5 10	5 18	5 32						
Tilt 17 ϕ =	30.39	36.90	45.57								
Scan time =	5 16	5 25	5 36								
Tilt 18 ϕ =	38.11	47.83									
Scan time =	5 39	5 52									
Tilt 19 ϕ =	48.85										
Scan time =	6 05										

vation angle increment between scans by 1.3 s deg^{-1}. By prorating the time increment for descent and finishing computations to each elevation scan, one has an estimate of how long a volume scan will take if the scan ends after an arbitrary number of tilts.

Listed in Table 1 are the elevation angles and cumulative scan times (minutes and seconds) for 11 potential VCPs. For a maximum height underestimate of 18%, there are 19 scans in 6.1 min, reaching a maximum elevation angle of 48.9°. At the other extreme, for 28%, there are 13 scans in 5.0 min, reaching a maximum elevation angle of 56.3°.

As an example of the advantages of the optimization technique, an optimized version of VCP 11 was produced. Optimized VCP 11 has the same lowest and highest elevation angles, the same number of elevation scans, and the same rotation rates as the original VCP 11. The optimized version of VCP 11 is shown in Fig. 3, where the maximum height underestimate is 19.34%. The optimized VCP provides better low elevation coverage at far ranges. Also, the more uniform distribution at higher elevation angles is quite evident. Shown in Fig. 4 are the jagged lines from Figs. 1 and 3, as well as the lines from three other heights, expressed as percent height underestimates. As expected, the height underestimates for optimized VCP 11 are much more consistent with height and range.

3. VCPs having improved vertical and temporal resolution

a. Flexible VCPs

Before proceeding, it is important to introduce the concepts of *flexible* and *inflexible* VCPs. An *inflexible* VCP is the type currently in use with the WSR-88D. Once the VCP is selected, it sequences through a set of elevation angles in a fixed amount of time. It does not matter whether there are storms at far ranges where there are no echoes above 7° elevation or whether storms are

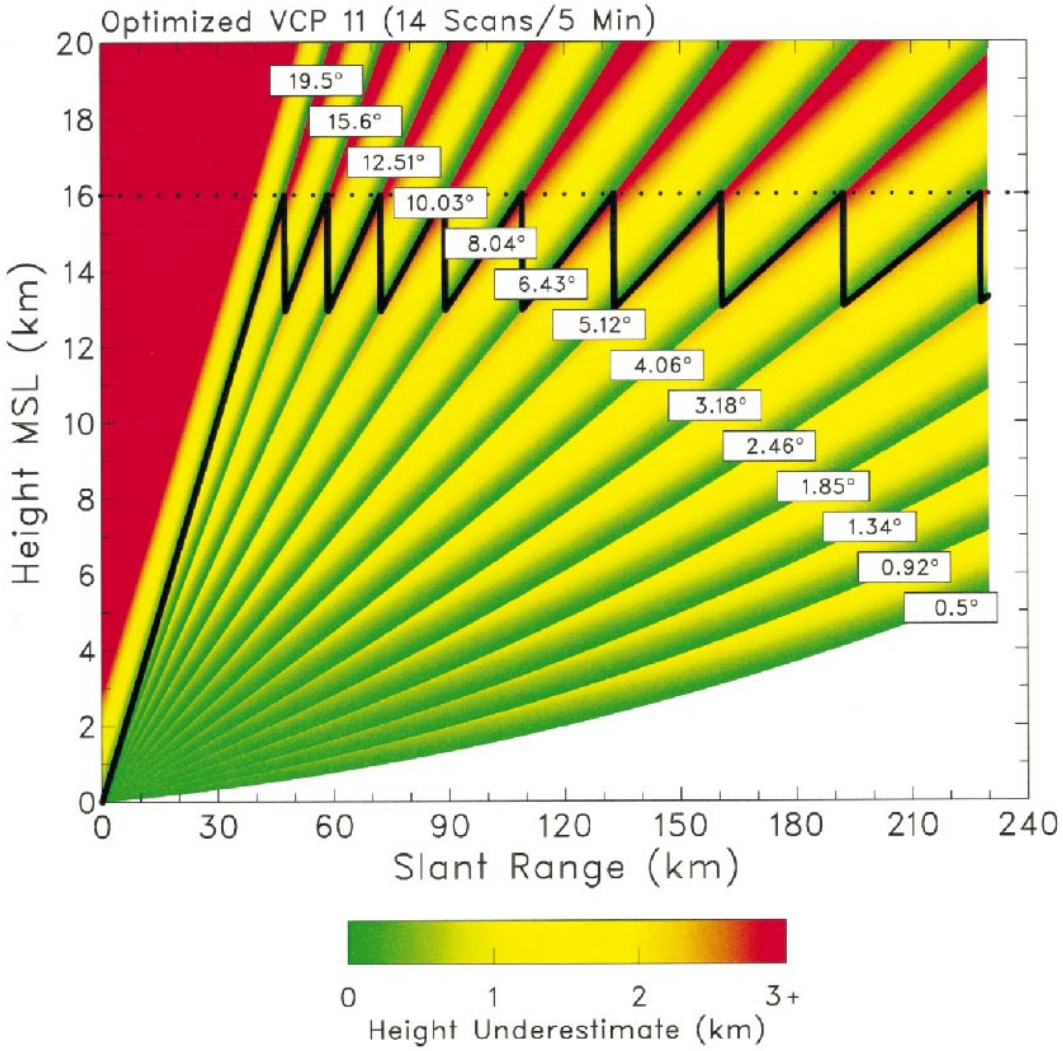

FIG. 3. Same as Fig. 1 except for optimized VCP 11.

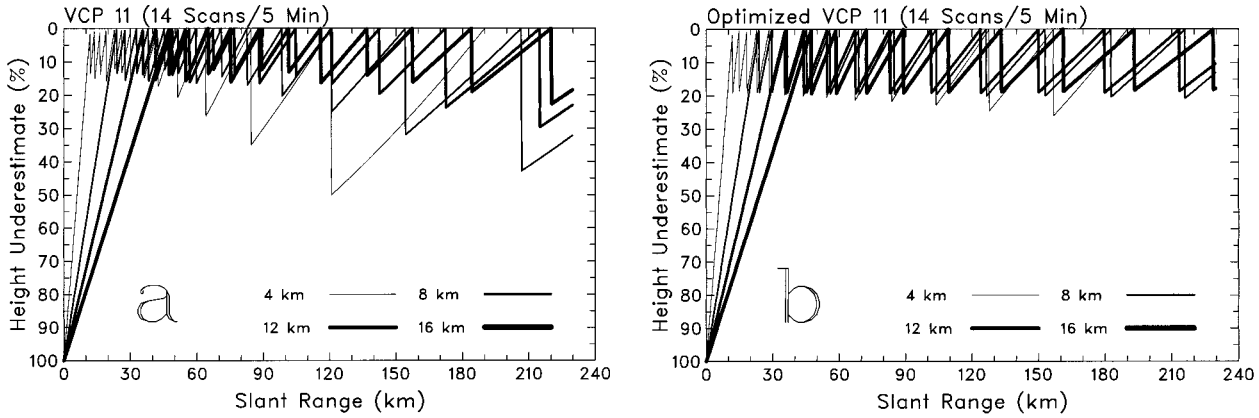

FIG. 4. Percentage height underestimates as a function of range for (a) VCP 11 and (b) optimized VCP 11. The jagged lines represent height underestimates at four different heights, including the height shown in Figs. 1 and 3.

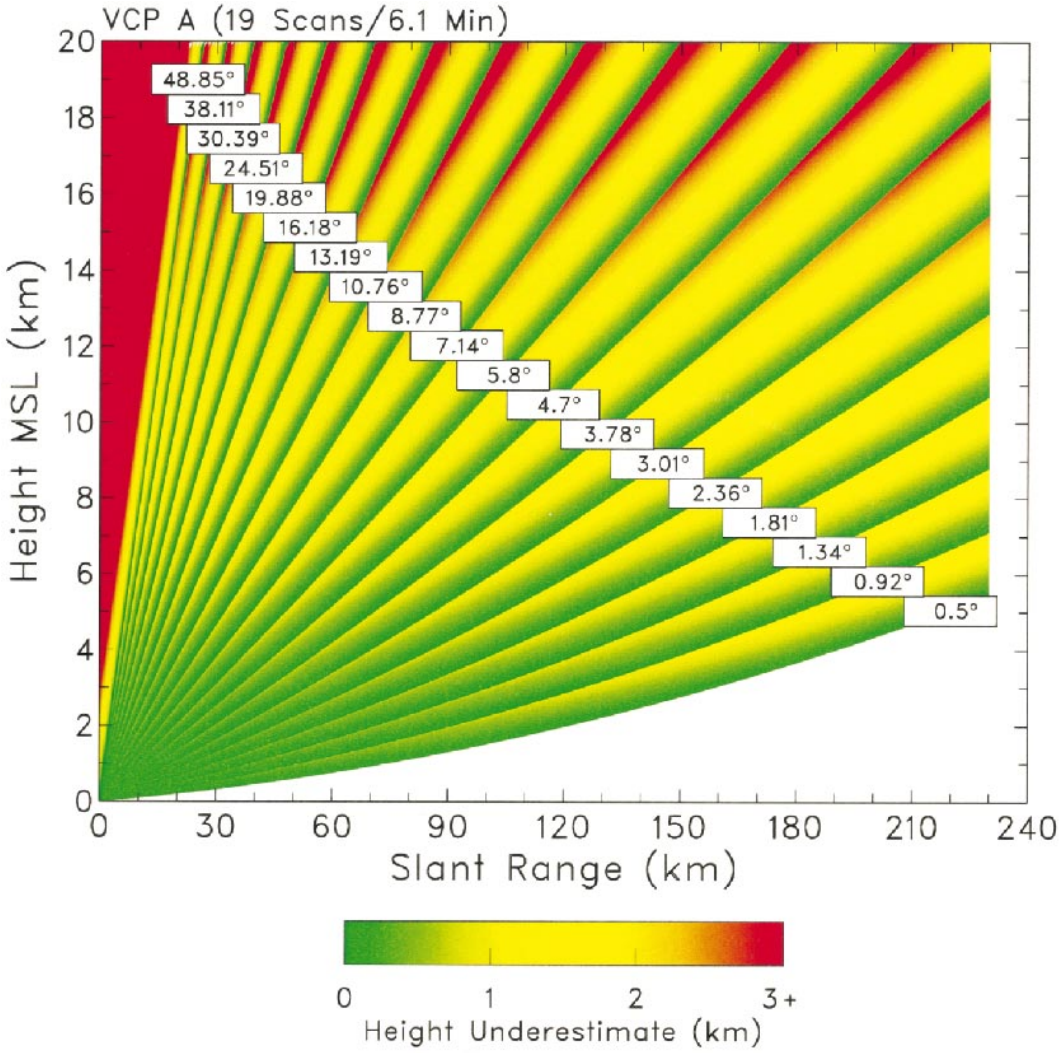

FIG. 5. Same as Fig. 1 except for VCP A.

passing over the radar. On the other hand, a *flexible* VCP allows an algorithm to specify when the VCP should end and start a new cycle. The algorithm would determine when there have been two successive scans with no radar return present above a threshold value. When that occurs, the volume scan automatically ends, provided that a minimum number of elevation scans have been completed. A new volume scan begins as soon as the antenna returns to the lowest elevation angle, and the end-of-volume-scan computations are completed. This approach was used successfully in the 1970s and 1980s for selected WSR-57 radars as part of the Digitized Radar (Saffle 1976) and the Radar Data Processor II experiments (Greene et al. 1983). The radar operator also should have the option to terminate the volume scan when situations dictate.

Temporal resolution is improved by having increased rotation rates and by not having to cycle through the entire volume scan. By the time that flexible VCPs with faster rotation rates are ready to be implemented on WSR-88Ds, the speed of the communication links should have accordingly increased to adequately handle the increased rate of data flow.

b. Development of prototype VCP A

From among the potential VCPs in Table 1, the one reaching the highest elevation in about 6 min, the same time as to complete VCP 21, was arbitrarily selected as VCP A. VCP A has a maximum height underestimate of 18% and consists of 19 scans that reach a maximum elevation angle of 48.9° (Fig. 5). This VCP helps to satisfy the users' needs for a reduced cone of silence to detect reflectivity features near the radar. Tall storms having *horizontal* ranges as close as 10–15 km to the radar are covered to storm top; horizontal range is approximately equal to slant range times the cosine of the elevation angle. With flexible capability, the radar com-

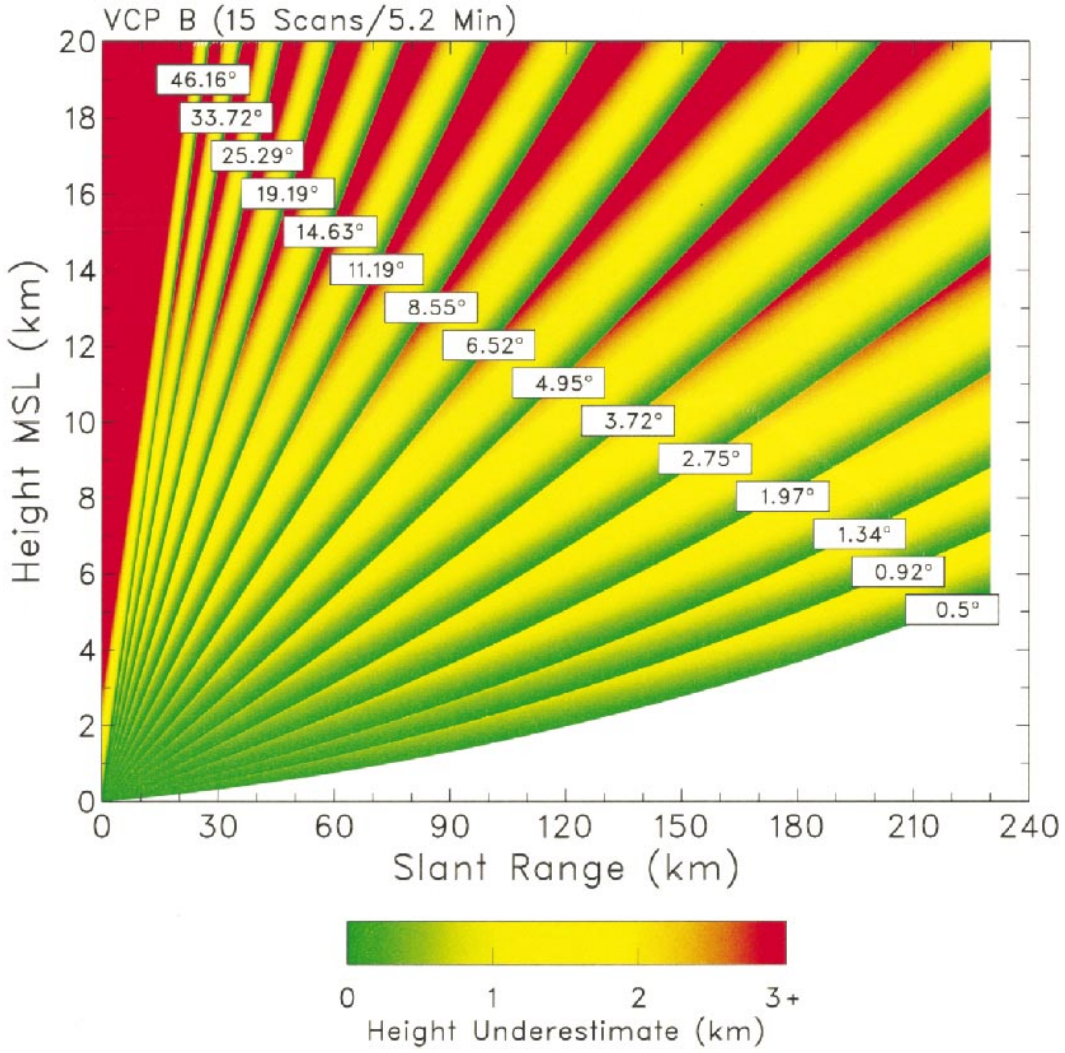

FIG. 6. Same as Fig. 1 except for VCP B.

pletes 16 scans in 5 min and reaches an elevation angle of 24.5°. Tall storms as close as approximately 35 km to the radar are covered to storm top with the 5-min sampling; short storms as close as about 20 km are covered. In 3.5 min, the radar completes 11 scans and reaches an elevation angle of 8.8°, which completely covers storms beyond 100 km. With 3.5-min sampling, rapidly evolving features in the lowest 3 km are covered as close as 20 km to the radar.

Besides the decreased cone of silence at near range, another advantage of VCP A is the increased vertical resolution at moderate to far ranges. Within the lowest 6° of elevation, VCP A has nine scans, compared to six for both VCPs 11 and 21. Within the lowest 3°, the average increment between elevation angles is 0.50°, compared with 0.95° for VCPs 11 and 21. The increased rotational speed of the radar's antenna makes possible the increased vertical resolution at all ranges. There will be a slight increase in spectrum width owing to the faster rotation rates (see appendix B).

c. Development of prototype VCP B

As a second example, the VCP in Table 1 that has a maximum height underestimate of 23% was chosen as VCP B. It consists of 15 scans that reach a maximum elevation angle of 46.2° in 5.2 min (Fig. 6). As with VCP A, this VCP scans to the top of tall storms at a horizontal range as close as 10–15 km to the radar. The vertical resolution of VCP B is coarser than that for VCP A and, accordingly, completes the full scan in 5.2 min instead of 6.1 min. The radar can sample phenomena as close as 20 km every 3.7 min if the phenomena are 5 km deep (highest elevation angle of 14.6°) and every 3.1 min if they are 3 km deep (highest elevation angle of 8.6°). The lowest elevation angle of 0.5° limits

TABLE 2. Approximate volume scan times (min) to reach specified elevation angles for various VCPs.

Elevation angle (°)	VCP 21	VCP 11	VCP A	VCP B
~45	—	—	6.1	5.2
~30	—	—	5.3	4.3–4.7
~20	6.0	5.0	4.6	4.0
~10	—	—	3.8	3.1

far-range detection of shallow phenomena. A more desirable lowest elevation angle would be 0.3° (Smith 1998).

VCPs A and B are arbitrary examples of the type of new scanning strategies that can satisfy the users' needs expressed in the introduction. They allow better vertical and temporal resolutions of tall phenomena at long ranges from a radar, as well as better vertical and temporal resolutions of shallow phenomena at close and moderate ranges. The improved vertical resolution permits better estimation of precipitation in shallow storms, such as hurricanes and winter storms. VCPs A and B lend themselves to better documentation of rapidly evolving features, such as tornadoes and downbursts. Further, they decrease the cone of silence, so that phenomena over populated areas located close to a radar can be detected. In order to implement these types of VCP changes, some of the WSR-88D algorithms need to be modified. Comparative volume scan times to reach specified elevation angles for VCPs 21, 11, A, and B are shown in Table 2.

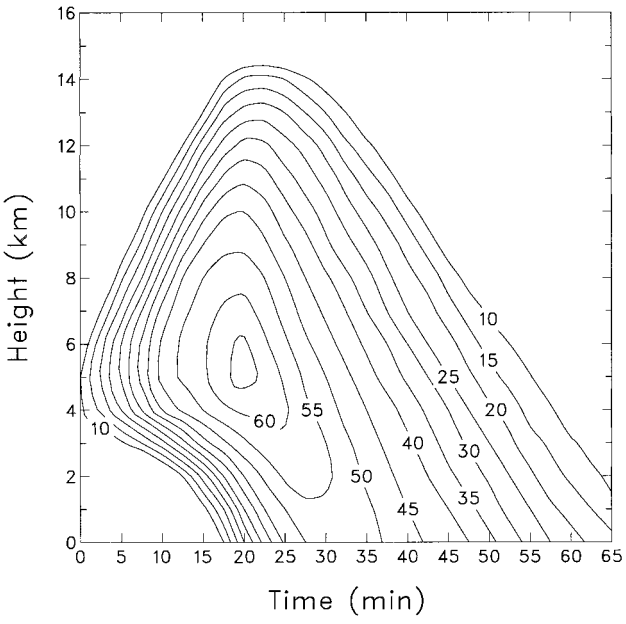

FIG. 7. Schematic time–height plot of maximum reflectivity (dBZ) within one cell of a multicell hailstorm. The schematic is based on a composite of data from an Alabama hail- and microburst-producing multicell storm (Kingsmill and Wakimoto 1991) and a North Dakota hail-producing multicell storm (Torgerson and Brown 1996).

4. Comparing optimized VCPs with VCPs 11 and 21

a. Testing improved vertical resolution

Vertically integrated liquid (VIL) is a computed quantity that forecasters use to estimate the severity of a storm. It is a measure of the liquid water in a vertical column in the storm and is computed as a function of the vertical profile of reflectivity (Greene and Clark 1972). Owing to its vertically integrated properties, VIL was selected for comparing the vertical resolution of the various VCPs.

A vertical profile of maximum reflectivity within an individual convective cell was used to compute VIL; VIL computed in this manner is called *cell-based* VIL. The profile was derived from the composite time–height evolution of reflectivity shown in Fig. 7. The composite was based on (a) data presented by Kingsmill and Wakimoto (1991) from an Alabama hail- and microburst-producing multicell storm and (b) data presented by Torgerson and Brown (1996) from a North Dakota hail-producing multicell storm. VIL was computed from the reflectivity profile at 20 min in Fig. 7. The true value of VIL for the profile, integrating over height intervals of 0.1 km, is 80.5 kg m^{-2}.

Figure 8 contains VIL values plotted as a function of range for VCPs 11 and 21, optimized VCP 11, and VCPs A and B. The VIL values based on VCP 21 are much more erratic than those for the other VCPs, fluctuating by up to 12–14 kg m^{-2} from the true value. This agrees with findings of Mahoney and Schaar (1993), who also pointed out the erratic behavior of VIL based on VCP 21. Within about 110 km of the radar, the VIL values for the other VCPs all fluctuate from -2 to $+4$ kg m^{-2} of the true value. At closer range, owing to the decreased cone of silence associated with VCPs A and B, realistic VIL values are computed to within 15 km of the radar, as opposed to 30–35 km for the other VCPs.

The increase in unrealistic VIL values beyond about 125 km is a consequence of the vertical distance between elevation angles, which increases with range. As part of the vertical integration process, the maximum reflectivity within the storm at each elevation angle is assigned to a height interval extending from halfway to the adjacent lower elevation angle to halfway to the adjacent higher elevation angle. So as the vertical distance between elevation angles increases with range, the height interval containing the largest reflectivity values

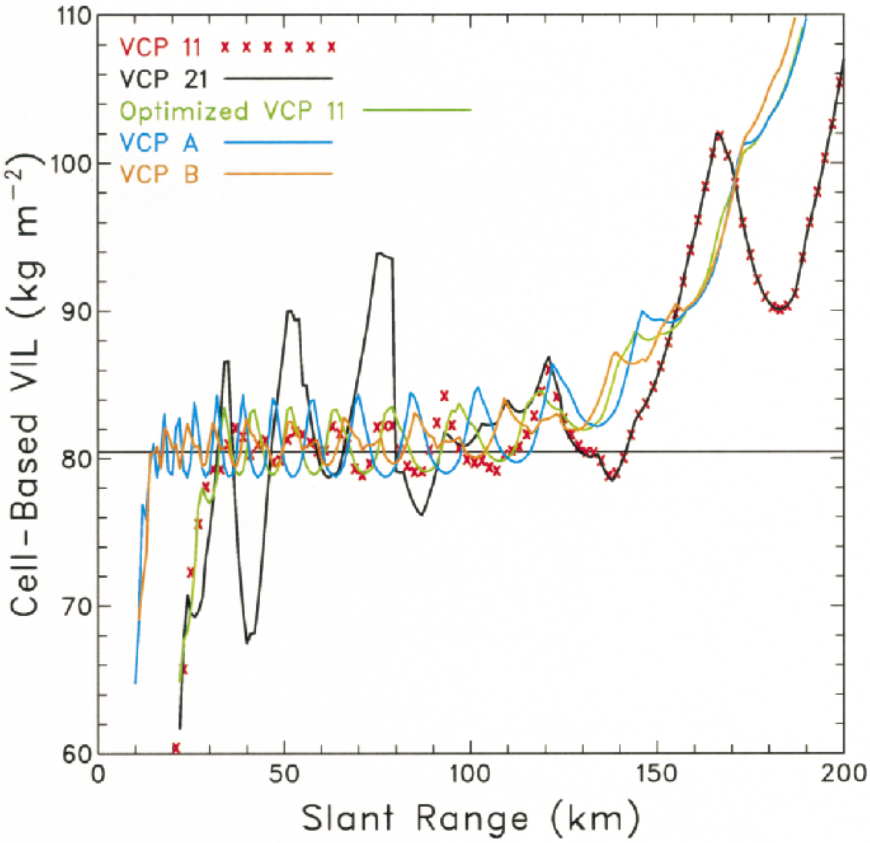

FIG. 8. VIL computed as a function of range based on the reflectivity composite in Fig. 7. The vertical reflectivity profile at 20 min (Fig. 7) was used for the computations. The horizontal line is the true VIL value of 80.5 kg m^{-2}.

carries an increasing amount of weight in computing the VIL value. Beyond about 125 km, the VCP 11 and 21 curves coincide because most of the storm depth is below 5.25°, where elevation angles are the same. In summary, VCPs A and B produce more consistent values of VIL than do VCPs 11 and 21 and produce realistic values at closer ranges than do VCPs 11 and 21.

b. Testing improved temporal resolution

One of the severe storm events that has a short lead time is the downburst. To develop a downburst model, the time–height profile of maximum reflectivity in Fig. 7 was used. In their study of microbursts (small-scale downbursts) in Colorado, Roberts and Wilson (1989) found that descending maximum reflectivity cores associated with midaltitude convergence are good indicators of a developing microburst. These signatures appeared 0–10 min before outflow winds occurred at the surface. Since midaltitude convergence information was not available, descent of the reflectivity core alone was used as the precursor signature of a downburst. Without much guidance, the precursor signature for a downburst was assumed to be the first detection of reflectivity descending faster than 3 m s^{-1}.

Using VCPs 11, 21, A, and B, the lead time was computed as a function of range. Lead time was defined as the difference between the time the precursor signature was first detected and the time that the reflectivity core reached the ground (32 min in Fig. 7). For flexible VCPs A and B, it was assumed that the volume scan terminated following the first elevation scan above 16-km height. The random temporal placement of a volume scan relative to the reflectivity features affects the value of the computed descent rate. To take into account the various random placements, the time interval between volume scans was divided into 10 equal parts and computed at nine additional lead times, each successively offset in time by one-tenth of the volume scan time interval.

Figure 9 shows the resulting lead times as a function of range for VCPs 11 and 21. The 10 dots, or horizontal lines, in the vertical at each range represent the 10 offset estimates of lead time for one volume scan. The lead time computed for a given volume scan is equally likely to be anywhere within the full spread of these lead times. The thick horizontal line indicates the time interval between volume scans (scale on the right); for these VCPs, the time interval remains constant with increasing range. There are no lead times beyond 200 km, owing to the

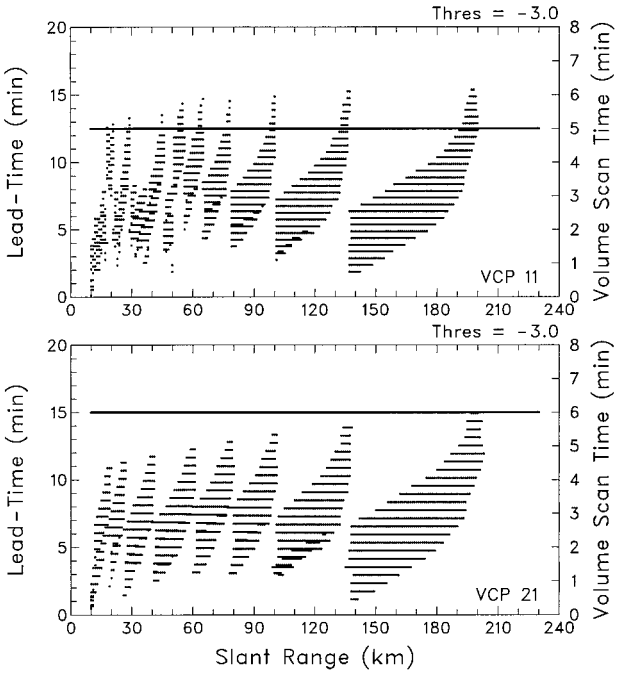

FIG. 9. Downburst lead times as a function of slant range for the reflectivity composite in Fig. 7 using VCP 11 (top) and VCP 21 (bottom). The set of 10 offset scans (10 dots or horizontal lines in the vertical at each range) is a proxy for all of the possible random placements of volume scans relative to the reflectivity core region. The thick line indicates the time it takes to complete one volume scan (scale on the right).

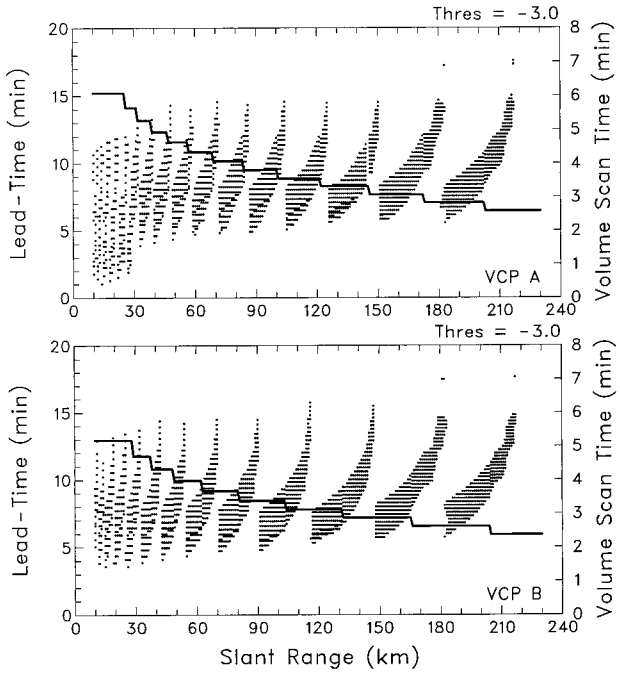

FIG. 10. Same as Fig. 9 except for VCP A (top) and VCP B (bottom).

lowest elevation angle being too high in the storm to detect the descent. The abrupt changes in lead time as a function of range arise from changes in the placement and vertical separation of the elevation angles relative to the height of the maximum reflectivities in the core region. Each contiguous set of dots/horizontal lines in the figure arises from a given pair of consecutive elevation angles between which the descent rate was computed. The variation in lead time at a given range, owing to the random location of a volume scan relative to the reflectivity core, is nearly equal to the time it takes to complete the respective VCP.

Figure 10 shows the lead times for optimized VCPs A and B. Being flexible VCPs, the time to complete a volume scan decreases with range because there is a decreasing number of elevation scans within storm depth. As the volume scan time decreases, the minimum lead time increases slightly and exhibits decreasing variation among the 10 offset volume scans at each range. The variations among the 10 offset scans for VCP A decrease from about 5.5 min at close range to 2.5 min at far range. Similar variations for VCP B decrease from about 4.5 min at close range to 2 min at far range.

The data presented in Figs. 9 and 10 clearly indicate that the average downburst lead times significantly increase at farther ranges with the reduced volume scan times that are possible with a flexible VCP. Even though the downburst is a low-altitude phenomenon that cannot be detected beyond about 75 km, the precursors occur aloft and, therefore, can be detected at much greater ranges from a radar. (Owing to the simple criterion used to compute lead time, one should compare only the trends, not the absolute values, of lead times in Figs. 9 and 10.)

5. Conclusions

When the WSR-88Ds were commissioned in the early and mid-1990s, the radars included two scanning strategies or volume coverage patterns for use with convective storms: VCP 11 (14 elevation scans to 19.5° in 5 min) and VCP 21 (9 elevation scans to 19.5° in 6 min). Since these VCPs were developed primarily for system development needs, radar users have found that the VCPs do not address meteorological needs in some storm situations.

VCP changes to improve vertical and temporal resolution of WSR-88D data in convective storms are proposed. Vertical resolution can be improved in two ways: 1) by providing more low elevation angles to improve sampling of distant storms and 2) by increasing the maximum elevation angle to improve sampling of storms near the radar. Temporal resolution can be improved in two ways. First, the antenna rotation rate can be increased to the maximum that is consistent with the desired accuracy of the data. Second, a volume scan can be terminated and recycled when the antenna tilts above all radar return or reaches a specified elevation angle.

Capabilities of the existing and proposed VCPs were

compared by producing simulated datasets based on a composite time–height cross section of maximum reflectivity within the typical cell of a multicell hailstorm. Vertically integrated liquid and downburst lead times were computed from the reflectivity cross section. Evaluations of these two quantities indicate that the types of new VCPs proposed here provide improved vertical and temporal resolution.

Acknowledgments. We appreciate comments on this manuscript by Ming Fang, Arthur Witt, and Dusan Zrnić of NSSL and by the two anonymous reviewers. Peggy Frazier provided valuable editorial advice. This study was funded primarily through a memorandum of understanding between NSSL and the WSR-88D Operational Support Facility.

APPENDIX A

Derivation of Optimized Elevation Angle

Following is the derivation of an equation for computing the elevation angle associated with a given height and slant range. According to Doviak and Zrnić (1993), the height of a radar beam, denoted by h, is given as

$$h = [(r'_e)^2 + r_s^2 + 2r_s r'_e \sin\phi]^{1/2} - r'_e, \quad \text{(A1)}$$

where r'_e is 6/5 the earth's radius (the value used with WSR-88Ds), r_s is the slant range, and ϕ is the elevation angle. To simplify (A1), a binomial expansion is used as given by

$$(1 + x)^n = 1 + nx + \frac{n(n-1)x^2}{2!} + \cdots, \quad \text{for } x^2 < 1. \quad \text{(A2)}$$

Rearranging the terms in (A1) and using $n = ½$ and ignoring second- and higher-order terms in (A2), (A1) reduces to

$$h = r_s \sin\phi + \frac{r_s^2}{2r'_e}. \quad \text{(A3)}$$

Replacing h by Z_t (true height) in (A3) and rearranging the terms, the new optimized elevation angle at height Z_t and slant range r_s can be computed from

$$\phi = \sin^{-1}\left(\frac{Z_t}{r_s} - \frac{r_s}{2r'_e}\right). \quad \text{(A4)}$$

APPENDIX B

Signal Statistics Related to Antenna Rotation Rate

Antenna speed affects radar signal statistics in two ways. The speed determines 1) the time available for spectral moment estimation over the 1° azimuthal interval between radials and 2) the amount of signal spectrum broadening owing to antenna motion. The effects of antenna speed are quantified in the following discussion.

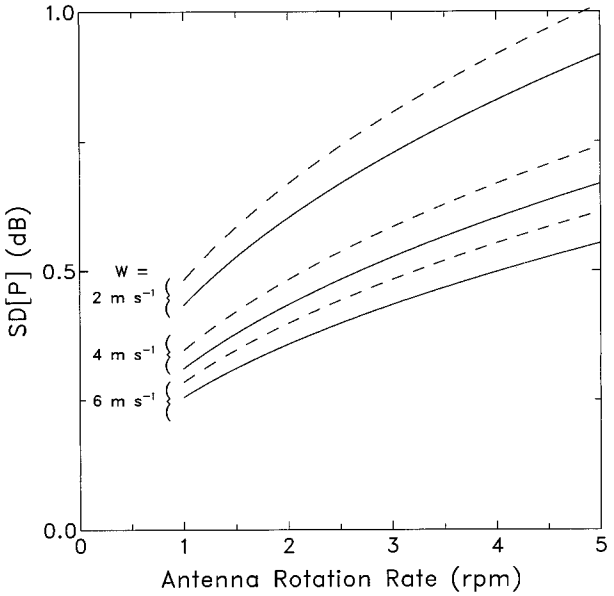

FIG. B1. Standard deviation of return power estimate (P) for 1° azimuthal samples as related to antenna rotation rate and spectrum width (W). Solid curve is contiguous sampling (estimate dwell of 1°), and dashed curve is batch sampling (estimate dwell of 0.8°).

a. Return power estimation

From a derivation given by Sirmans and Doviak (1973), the standard deviation (SD) of the return power estimate (P, dB) at signal-to-noise ratios greater than 8 dB can be expressed as

$$\mathrm{SD}(P) = 10 \log\left[1 + \frac{1}{(16\sqrt{\pi}MT_sW/\lambda)^{1/2}}\right], \quad \text{(B1)}$$

where λ is radar wavelength (m), T_s is radar time sampling interval (or pulse repetition time, PRT, in s), W is Doppler velocity spectrum width (m s^{-1}), M is number of samples in the estimate, and MT_s is dwell time (s) for the estimate.

The standard deviation for the WSR-88D median wavelength and dwell time for 1° azimuthal sampling is shown in Fig. B1. Note that the standard deviation of power decreases with increasing spectrum width and dwell time and is 1 dB or less at any allowable rotation rate (<5 rpm or 30° s^{-1}) and the range of parameters shown. The spectrum width values represented by the curves in the figure are those expected to be found in convective storms.

b. Spectral broadening owing to antenna motion

From the derivation given by Nathanson (1969), the width (or standard deviation) of the Doppler velocity

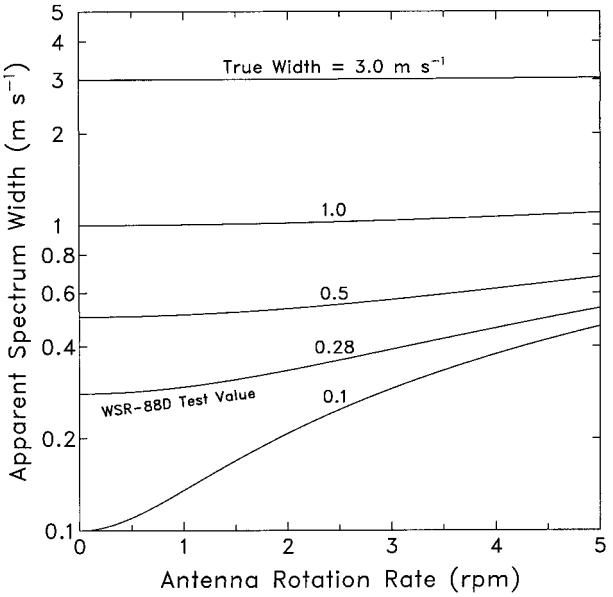

FIG. B2. Spectral broadening due to antenna motion at median frequency and beamwidth. ''WSR-88D test value'' is the best estimate of ground clutter average width. At low elevation angles, changes in rotation rate from 3.1–3.2 rpm for VCP 11 to 3.5–4.0 rpm for VCP A and B have little effect on clutter filter performance.

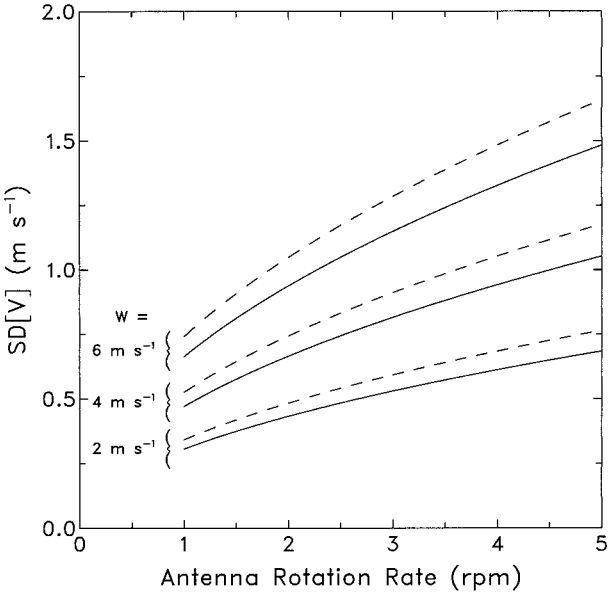

FIG. B3. Standard deviation of Doppler velocity estimate for 1° samples as related to antenna rotation rate and spectrum width (W). Solid curve is contiguous sampling (estimate dwell of 1°), and dashed curve is batch sampling (estimate dwell of 0.8°). Pulse repetition time is 0.986 ms (maximum unambiguous velocity is 26.5 m s^{-1} at median wavelength), the largest of the original WSR-88D PRTs (worst case standard deviation).

spectrum due to antenna motion (σ_m, m s^{-1}) can be expressed as

$$\sigma_m = \frac{\lambda\alpha}{10.7\theta_2}, \tag{B2}$$

where α is antenna rotation rate (° s^{-1}), and θ_2 is antenna two-way half-power beamwidth (°). For the WSR-88D median wavelength of 10.46 cm, median two-way half-power beamwidth of 0.65°, and rotation rate in revolutions per minute (rpm), Eq. (B2) reduces to

$$\sigma_m = \frac{\text{rpm}}{11}, \tag{B3}$$

where σ_m is still expressed in meters per second. Because broadenings due to antenna rotation (σ_m^2) and motion of scatterers (σ_T^2) are uncorrelated and additive, the apparent spectrum width (σ_a) is

$$\sigma_a = (\sigma_m^2 + \sigma_T^2)^{1/2}. \tag{B4}$$

Spectral broadening as related to antenna rotation rate is shown in Fig. B2. The curves in the figure indicate that for spectrum widths associated with meteorological phenomena (>1 m s^{-1}) and for allowable rotation rates (<5 rpm, 30° s^{-1}), spectral broadening owing to antenna rotation is negligible. The WSR-88D automatically increases the clutter filter notch width with an increasing rotation rate unless overridden by manual selection of filter parameters.

c. Doppler velocity estimation

From the derivation given by Zrnić (1977), the standard deviation of the Doppler velocity estimate for signal-to-noise ratios greater than 8 dB can be expressed as

$$\text{SD}(V) = \frac{\lambda}{2}\sqrt{\frac{w}{4\sqrt{\pi}\beta^2(T_s)MT_s}}, \tag{B5}$$

where w is Doppler frequency spectrum width (Hz), which is equal to $2W$ (m s^{-1})/λ, and

$$\beta(T_s) = \exp(-2\pi^2 w^2 T_s^2) \tag{B6}$$

is the signal correlation function for Gaussian spectra. The standard deviation for the WSR-88D median wavelength, sampling interval of 0.986 ms, and a 1° azimuthal dwell time is shown in Fig. B3. The standard deviation of velocity is directly proportional to the square root of spectrum width, inversely proportional to square root of dwell time, and is generally less than 1 m s^{-1} at the benchmark width of 4 m s^{-1} for any rotation rate.

REFERENCES

Brown, R. A., J. M. Janish, and V. T. Wood, 2000: Impact of WSR-88D scanning strategies on severe storm algorithms. *Wea. Forecasting,* **15,** 90–102.

Doviak, R. J., and D. S. Zrnić, 1993: *Doppler Radar and Weather Observations.* Academic Press, 562 pp.

Greene, D. R., and R. A. Clark, 1972: Vertically integrated liquid: A new analysis tool. *Mon. Wea. Rev.,* **100,** 548–552.

——, J. D. Nilsen, R. E. Saffle, D. W. Holmes, M. D. Hudlow, and P. R. Ahnert, 1983: RADAP II, an interim radar data processor. Preprints, *21st Conf. on Radar Meteorology,* Edmonton, AB, Canada, Amer. Meteor. Soc., 404–408.

Howard, K. W., J. J. Gourley, and R. A. Maddox, 1997: Uncertainties in WSR-88D measurements and their impacts on monitoring life cycles. *Wea. Forecasting,* **12,** 166–174.

Kingsmill, D. E., and R. M. Wakimoto, 1991: Kinematic, dynamic, and thermodynamic analysis of a weakly sheared severe thunderstorm over northern Alabama. *Mon. Wea. Rev.,* **119,** 262–297.

Maddox, R. A., D. S. Zaras, P. L. MacKeen, J. J. Gourley, R. Rabin, and K. W. Howard, 1999: Echo height measurements with the WSR-88D: Use of data from one versus two radars. *Wea. Forecasting,* **14,** 455–460.

Mahoney, E. A., and R. Schaar, 1993: WSR-88D scan strategy impacts on the vertically integrated liquid product. Preprints, *26th Int. Conf. on Radar Meteorology,* Norman, OK, Amer. Meteor. Soc., 44–46.

Nathanson, F. E., 1969: *Radar Design Principles.* McGraw-Hill, 626 pp.

OFCMSSR, 1991: Doppler radar meteorological observations. Part C: WSR-88D products and algorithms. Federal Meteorological Handbook 11, FCM-H11C-1991, 202 pp. [Available from Office of the Federal Coordinator for Meteorological Services and Supporting Research, Rockville, MD 20852.]

Roberts, R. D., and J. W. Wilson, 1989: A proposed microburst nowcasting procedure using single-Doppler radar. *J. Appl. Meteor.,* **28,** 285–303.

Saffle, R. E., 1976: D/RADEX products and field operation. Preprints, *17th Conf. on Radar Meteorology,* Seattle, WA, Amer. Meteor. Soc., 555–559.

Sirmans, D., and R. J. Doviak, 1973: Meteorological radar signal intensity estimation. NOAA Tech. Memo. ERL NSSL-64, National Severe Storms Laboratory, Norman, OK, 80 pp. [NTIS COM-73-11923/2AS.]

Smith, P. L., 1998: On the minimum useful elevation angle for weather surveillance radar scans. *J. Atmos. Oceanic Technol.,* **15,** 841–843.

Torgerson, K. L., and R. A. Brown, 1996: Radar signatures of updrafts within the Carson, ND hailstorm of 11 July 1989. Preprints, *18th Conf. on Severe Local Storms,* San Francisco, CA, Amer. Meteor. Soc., 81–85.

Zrnić, D. S., 1977: Spectrum moment estimates from correlated pulse pairs. *IEEE Trans. Aerosp. Electron. Syst.,* **AES-13,** 344–354.